Electronic Supplementary Material (ESI) for Dalton Transactions.
This journal is © The Royal Society of Chemistry 2017

Supporting Information

A Luminescent Pt_2Fe Spin Crossover Complex

Bernhard Schäfer,[1] Thomas Bauer,[2] Isabelle Faus,[2] Juliusz A. Wolny[2] Fabian Dahms,[2] Olaf Fuhr,[1,3] Sergei Lebedkin,[1] Hans-Christian Wille,[5] Kai Schlage,[5] Katharina Chevalier,[2] Fabian Rupp,[2] Rolf Diller,[2] Volker Schünemann,[2] Manfred M. Kappes,[1,4] Mario Ruben[1,6*]

Mario.Ruben@kit.edu

1) Institut für Nanotechnologie, Karlsruher Institut für Technologie (KIT), Campus Nord, Hermann-von-Helmholtz-Platz 1, 76344 Eggenstein-Leopoldshafen, Germany.
2) Fachbereich Physik, Technische Universität Kaiserslautern (TUK), Erwin-Schrödinger-Straße 46, 67663 Kaiserslautern, Germany.
3) Karlsruhe Nano-Micro Facility (KNMF), Karlsruher Institut für Technologie (KIT), Campus Nord, Hermann-von-Helmholtz-Platz 1, 76344 Eggenstein-Leopoldshafen, Germany.
4) Institut für Physikalische Chemie, Karlsruher Institut für Technologie (KIT), Fritz-Haber-Weg 2, 76131 Karlsruhe, Germany.
5) P01, Petra III, DESY (member of the Helmholtz Association (HGF), Notkestraße 85, 22607 Hamburg, Germany.
6) Institut de Physique et Chimie des Matériaux de Strasbourg (IPCMS), CNRS-Université de Strasbourg, 23, rue du Loess, BP 43, 67034 Strasbourg cedex 2, France.

Table of content

Table S1: Chrystal data and structure refinement for crystals of $\mathbf{1^H}$, $\mathbf{1^L}$, and **L-Pt**

Compound	$\mathbf{1^H}$	$\mathbf{1^L}$	**L-Pt**
Moiety formula	$[(C_{40}H_{43}N_8Pt)_2Fe](BF_4)_4 \cdot 3.5CH_2Cl_2$	$[(C_{40}H_{43}N_8Pt)_2Fe](BF_4)_4 \cdot 10CH_2Cl_2$	$[(C_{40}H_{43}N_8Pt)](PF_6) \cdot 2CH_3CN$ [1)]
Empirical formula	$C_{83.5}H_{91}B_4Cl_7F_{16}FeN_{16}Pt_2$	$C_{90}H_{106}B_4N_{16}F_{16}FePt_2Cl_{20}$	$C_{44}H_{49}F_6N_{10}PPt$ [1)]
M [g mol^{-1}]	2360.14	2914.17	1057.98 [1)]
Crystal colour	orange	red	yellow
T [K]	180.2	180.2	180.2
λ [Å] (MoKα)	0.71073	0.71073	0.71073
Crystal system	triclinic	monoclinic	monoclinic
space group	$P\bar{1}$	$C2/c$	$P2_1/m$
a [pm]	1633.44(3)	32.6480(8)	1731.99(10)
b [pm]	1720.29(4)	19.9969(5)	676.00(3)
c [pm]	1859.45(4)	17.9521(4)	2165.83(12)
α [°]	92.483(2)	90	90
β [°]	114.560(2)	97.533(2)	113.216(4)
γ [°]	90.524(2)	90	90
V [Å^3]	4745.73(17)	11619.0(5)	2330.5(2)
Z	2	4	2
$\rho_{calcd.}$ [g cm^{-3}]	1.652	1.666	1.508
μ(Mo-K_α) [mm^{-1}]	3.372	3.061	3.107
F(000)	2338	5776.0	1016
Crystal size [mm]	0.16 x 0.14 x 0.05	0.31 × 0.27 × 0.14	0.19 x 0.18 x 0.07
2θ range for data coll. [°]	2.80 to 51.36	4.29 to 51.43	5.12 to 51
Reflections collected	36901	30271	9533
Independent reflections	17702 [R_{int} = 0.0461, R_σ = 0.0643]	10901 [R_{int} = 0.0438, R_σ = 0.0325]	4574 [R_{int} = 0.0311, R_σ = 0.0267]
Ind. Reflections with $I \geq 2\sigma(I)$	12923	9322	4322
Data/restraints/parameters	17702/84/1140	10901/8/682	4574/3/338
Final R indices ($I \geq 2\sigma(I)$)	R_1 = 0.0532, wR_2 = 0.1231	R_1 = 0.0570, wR_2 = 0.1609	R_1 = 0.0490, wR_2 = 0.1254
Final R indices (all data)	R_1 = 0.0807, wR_2 = 0.1341	R_1 = 0.0647, wR_2 = 0.1695	R_1 = 0.0525, wR_2 = 0.1273
GoF on F_2	0.997	1.026	1.102
Largest diff. peak/hole / e Å^{-3}	2.64/–1.20	2.03/–1.60	3.70/–1.47
CCDC number	1510868	1510869	1510870

[1] During the refinement process one acetonitrile molecules could be localised and refined. The electron density in the remaining voids could not be assigned properly. Therefor their contribution was subtracted from the electron density map and a modified hkl file was calculated using the SQUEEZ algorithm provided by the program package PLATON.[1] By this method two solvent accessible voids (each approx. 155 Å^3) were calculated each containing approx. 18 electros which may represent one acetonitrile molecule. This finally results in the given formula of 2 molecules of acetonitrile per formula unit which was also considered in the given molecular weight.

[1] A.L. Spek, J. Appl. Cryst. 36 (2003) 7-13; A.L. Spek, Acta Cryst. D65 (2009) 148-155.

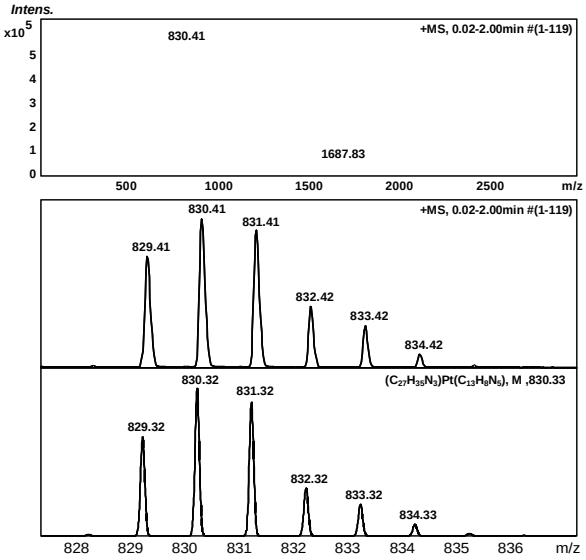

Figure S1. top: ESI-TOF mass spectrum of **L-Pt** sprayed from CH_3CN, middle: $[M–BF_4]^+$ peak m/z = 830.3, and bottom: the theoretical isotope pattern

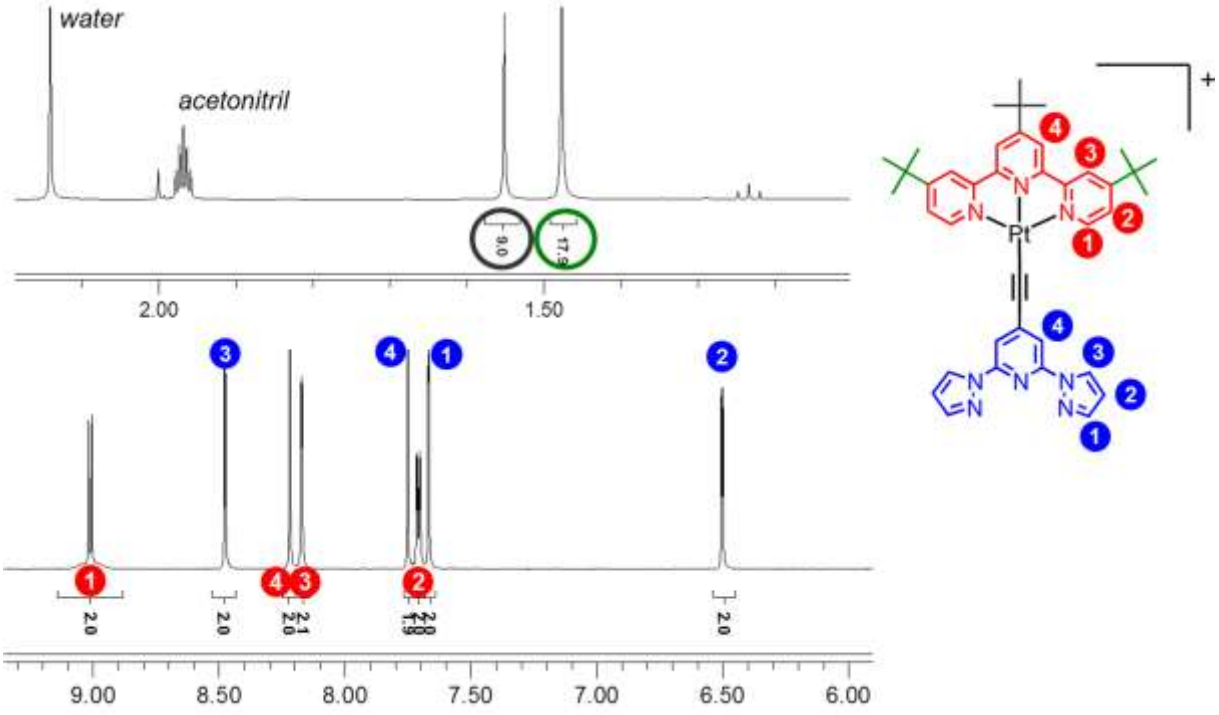

Figure S2. ^1H NMR spectrum of **L-Pt** in CD_3CN solution and peak assignment

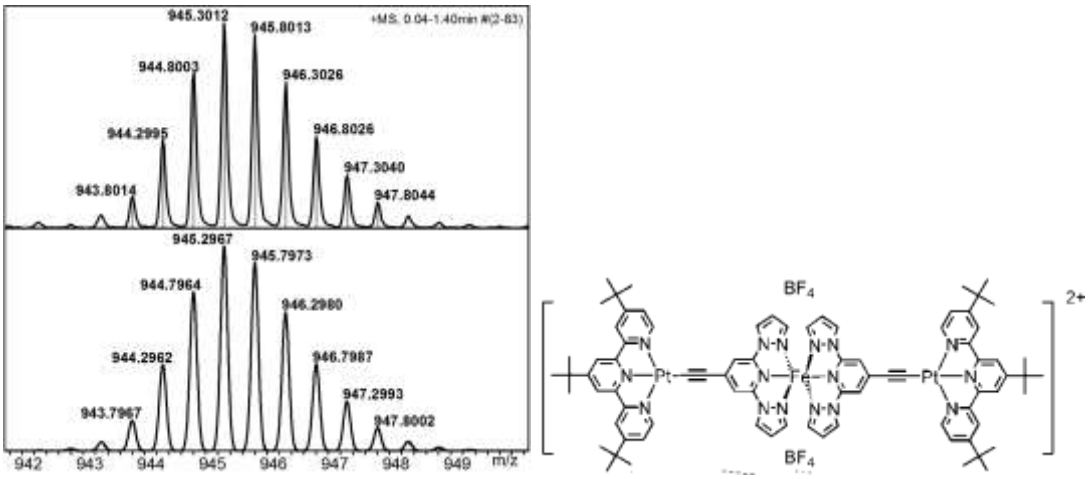

Figure S3 left: experimental (top) and theoretical (bottom) isotopic patterns of [**1**-2BF_4]$^{2+}$ and right: the respective structural formula; the compound was sprayed from CH_3CN in this ESI-TOF mass spectrometry experiment, the peak was of low intensity and the concentration had to be increased to concentrations higher then 1E-4mol/L

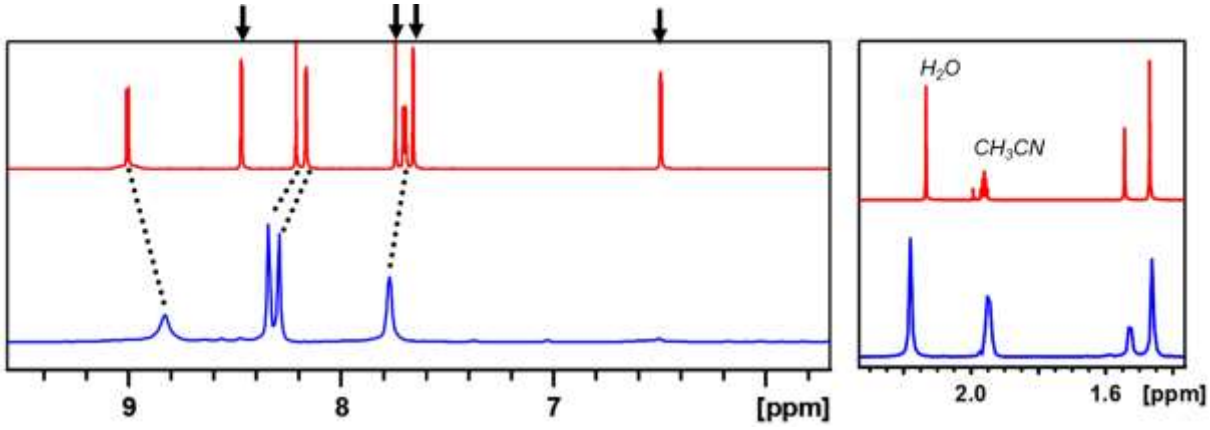

Figure S4 Comparison of the ^{1}H NMR spectra of **L-Pt** (top, red) and **1** (bottom, blue) in CD_3CN; the bpp-based resonances marked with black arrows (in the spectrum of **L-Pt**, top) are shifted to lower fields experiencing the paramagnetic character of the coordinated Fe^{II} ion in **1**, the tbbpy-based resonances are broadened in the spectrum of **1**;

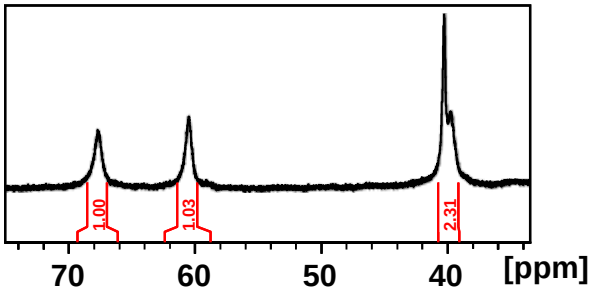

Figure S5 Upon coordination of Fe^{II} the bpp-based resonances are low-field shifted and can be found between 40 and 70 ppm in the ^{1}H NMR spectrum of **1** (in CD_3CN)

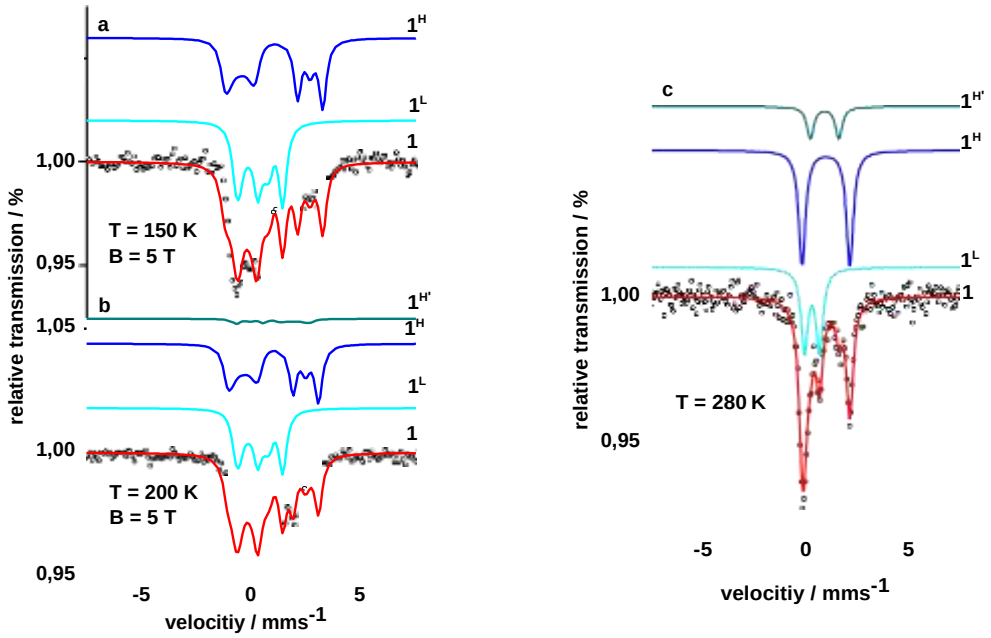

Figure S6 a) Mössbauer spectra of **1** taken at T=150 K (a) and T=200 K (b) with an applied external field of B=5 T. At such temperatures the fine structure levels of the HS site are almost equally populated and fast spin relaxation between the sublevels leads to a quasi-diamagnetic Mössbauer pattern which allows to determine the sign of the quadrupole splitting. This characteristic pattern shows a negative sign for the quadrupole splitting of component $\mathbf{1}^{H}$ without asymmetry. The solid lines are simulations according to the Spin-Hamiltonian formalism calculated under assumption of fast relaxation, with the parameters presented in table 2 of the main manuscript, except a slight modification of the isomer shift and the quadrupole splitting due to thermal shifts for the HS site: a) δ_1=1.09 mms^{-1}, ΔE_{Q1}=-3.17 mms^{-1}; b) δ_1=1.05 mms^{-1}, ΔE_{Q1}=-2,84 mms^{-1}. In b) we have added a new component $\mathbf{1}^{H'}$ (4 % spectral contribution), as a result of thermal SCO from $\mathbf{1}^{L}$ to $\mathbf{1}^{H'}$ as indicated from low field Mössbauer spectroscopy (not shown). Component $\mathbf{1}^{H'}$ shows δ_3=0.98 mms^{-1} ΔE_{Q3}=(±) 2.01 mms^{-1}. The line width for all components is Γ=0.40 mms^{-1}. c) Mössbauer spectra of **1** measured at T=280 K and fitted with Lorentzian doublets: Component $\mathbf{1}^{L}$ shows a loss in percental share of 14 % and a new component $\mathbf{1}^{H'}$ arises with 15 % relative contribution. Component $\mathbf{1}^{H}$ stays with 50 % and exhibits δ_2=1.01 mms^{-1} as a consequence of second-order Doppler shift and ΔE_{Q2}=(-)2.33 mms^{-1}. The SCO component $\mathbf{1}^{H'}$ has δ_3=0.94 mms^{-1} and ΔE_{Q3}=1.39 mms^{-1}. The 300K measurement has been taken in continuous flow cryostat from Oxford Instruments. The line width was Γ=0.40 mms^{-1}.

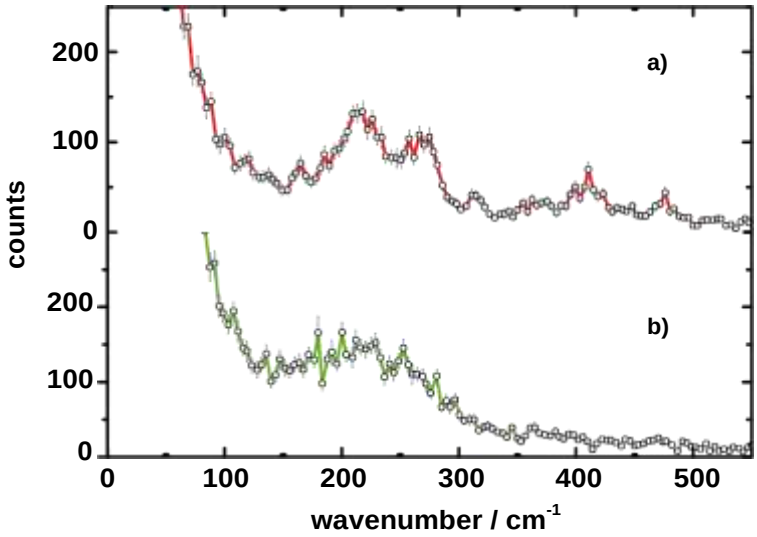

Figure S7 Experimentally determined NIS data of **1** obtained at a) 80 K and b) 300 K. This data has been used to calculate the pDOS displayed in Figure 6a and b.

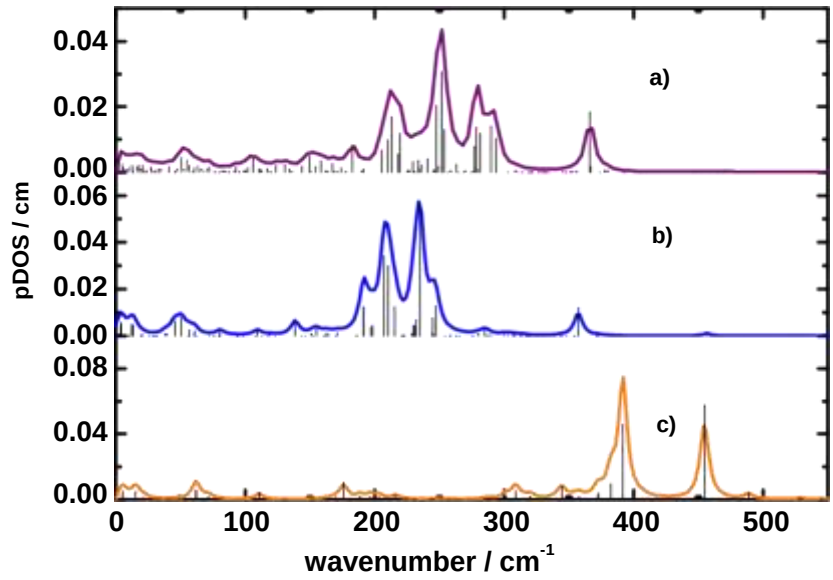

Figure S8 DFT-calculated pDOS of the single components used in the simulations presented in Fig. 6c and d: a) Calculated pDOS based on the structural input $\mathbf{1}^{H}$ representing the HS iron which is trapped in the HS state and does not undergo SCO; b) calculated pDOS of molecules which have switched from LS to HS ($\mathbf{1}^{H'}$) by retaining the straight molecular structure of $\mathbf{1}^{L}$; c) calculated pDOS based on the structural input $\mathbf{1}^{L}$ representing the LS iron which is capable of SCO. DFT calculations have been performed using Gaussian 09 Rev. D.01 (B3LYP/CEP31-G). The vertical lines highlight the quadratic displacement of the iron atoms within a particular mode.

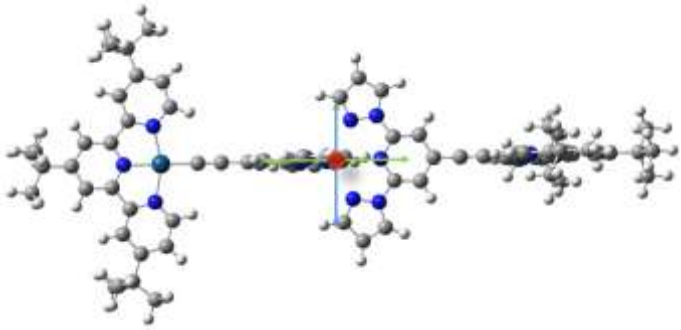

Figure S9 Graphic visualization of the DFT minimized structure of complex $\mathbf{1}^{L}$. The main three axes of the iron atom movement are visualized by arrows. The green arrow represents movement along the axis between the platinum atoms (PPA). The blue (and red) arrows visualize iron movement perpendicular to the Pt-Pt axes, here either out of the plane (OOP) or in the plane vertical to the Pt atoms (IPV).

Table S2 Presentation of characteristic modes obtained by DFT simulations of the pDOS of **1** displayed in Fig. 6 c and d. The table shows the calculated mode energies, the type of iron movement of the molecular mode, the spin state of the iron centre (with the type of optimized structure in brackets) and the file names of the corresponding visualizations given also as supplementary material. The movie files of the type movie.gif can be played *e.g.* with the MS internet explorer.

E [cm^{-1}]	type of vibration	iron spin state	movie
191.3	OOP	HS ($\mathbf{1}^{H'}$)	FePt_HS_191a
191.6	IPV	HS ($\mathbf{1}^{H'}$)	FePt_HS_191b
207.0	OOP+IPV	HS ($\mathbf{1}^{H'}$)	FePt_HS_207
205.5	OOP+IPV	HS ($\mathbf{1}^{H}$)	FePt_trapped_HS_205
210.0	OOP+IPV	HS ($\mathbf{1}^{H}$)	FePt_trapped_HS_210
210.5	OOP+IPV	HS ($\mathbf{1}^{H'}$)	FePt_HS_210
213.2	IPV	HS ($\mathbf{1}^{H}$)	FePt_trapped_HS_213
215.4	PPA	HS ($\mathbf{1}^{H'}$)	FePt_HS_215
218.1	OOP+IPV+PPA	HS ($\mathbf{1}^{H}$)	FePt_trapped_HS_218
219.6	OOP+IPV+PPA	HS ($\mathbf{1}^{H}$)	FePt_trapped_HS_219
234.9	PPA	HS ($\mathbf{1}^{H'}$)	FePt_HS_234
244.7	OOP+IPV	HS ($\mathbf{1}^{H'}$)	FePt_HS_244
247.2	OOP+IPV	HS ($\mathbf{1}^{H'}$)	FePt_HS_247
247.4	IPV	HS ($\mathbf{1}^{H}$)	FePt_trapped_HS_247
251.8	OOP+IPV	HS ($\mathbf{1}^{H}$)	FePt_trapped_HS_251
253.7	OOP+IPV	HS ($\mathbf{1}^{H}$)	FePt_trapped_HS_253
277.0	IPV+PPA	HS ($\mathbf{1}^{H}$)	FePt_trapped_HS_277
278.5	IPV+PPA	HS ($\mathbf{1}^{H}$)	FePt_trapped_HS_278
281.3	PPA	HS ($\mathbf{1}^{H}$)	FePt_trapped_HS_281
289.9	OOP+PPA	HS ($\mathbf{1}^{H}$)	FePt_trapped_HS_289
293.8	PPA	HS ($\mathbf{1}^{H}$)	FePt_trapped_HS_293
308.8	OOP+IPV	LS ($\mathbf{1}^{L}$)	FePt_LS_308
357.2	PPA	HS ($\mathbf{1}^{H'}$)	FePt_HS_357
366.1	PPA	HS ($\mathbf{1}^{H}$)	FePt_trapped_HS_366
382.4a	OOP+IPV	LS ($\mathbf{1}^{L}$)	FePt_LS_382a
382.4b	OOP+IPV	LS ($\mathbf{1}^{L}$)	FePt_LS_382b
391.6a	OOP+IPV	LS ($\mathbf{1}^{L}$)	FePt_LS_391a
391.6b	OOP+IPV	LS ($\mathbf{1}^{L}$)	FePt_LS_391b
454.6	PPA	LS ($\mathbf{1}^{L}$)	FePt_LS_454

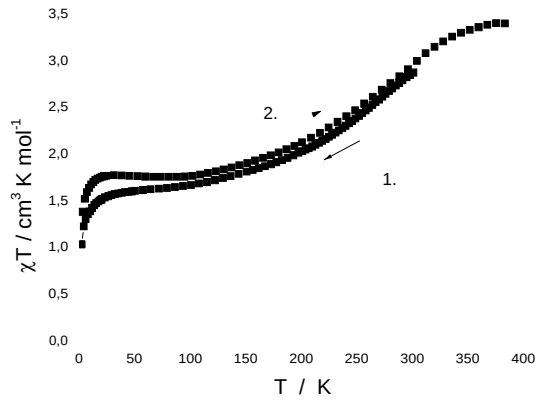

Figure S10 Magnetic properties of compound **1**, χT plot (B=0.1 T), shown is the first cooling-heating cycle

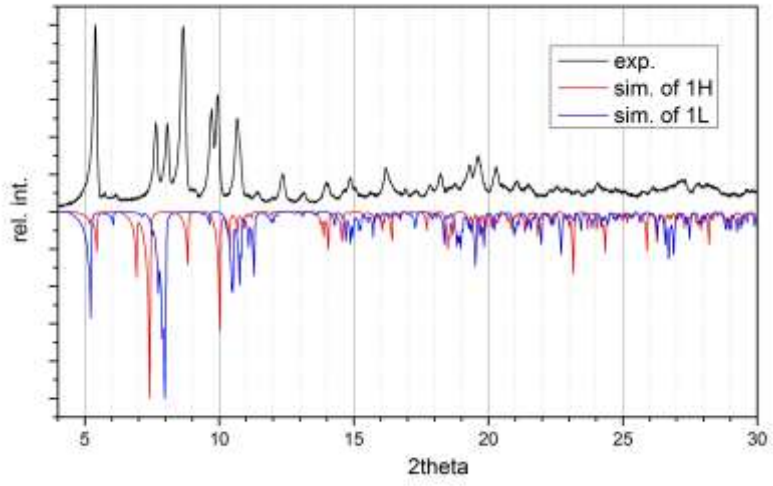

Figure S11 Comparison of the powder diffraction data of the powder with the calculated patterns of $\mathbf{1^L}$ and $\mathbf{1^H}$ indicates that the crystalline integrity of the powder was lost after solvent liberation of the co-crystalized CH_2Cl_2

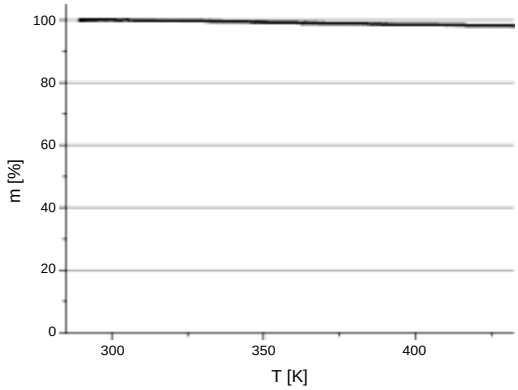

Figure S12 Thermogravimetric analysis of the powder sample of **1**, which was stored under a stream of argon until weight constancy was achieved (before analysis).

Table S3. Structural data for $\mathbf{1}^{H}$, $\mathbf{1}^{L}$, and $[Fe(bpp)_2][BF_4]_2$ (for comparison). See the main text of [Chem. Soc. Rev., 2011, **40**, 4119–4142] for the definitions of the four distortion parameters. Data of $[Fe(1\text{-}bpp)_2][BF_4]_2$ is from Coord. Chem. Rev., 2009, **253**, 2493.

	Spin-state behaviour	Spin-state of Crystal structure	θ (°)	ϕ (°)	Σ (°)	Θ (°)
$\mathbf{1}^{L}$	Spin-crossover	Low-spin	77.14	179.42	94	275
$\mathbf{1}^{H}$	High-spin	High-spin	75.20	156.75	169	522
$[Fe(1\text{-}bpp)_2][BF_4]_2$	Spin-crossover	High-spin	89.94	172.98	150.8	467
		Low-spin	89.40	178.15	86.1	282